Chapter 14

Microelectrode Measurements in Stromatolites: Unraveling the Earth's Past?

Pieter T. Visscher[1,*], Shelley E. Hoeft[1], Tonna-Marie L. Surgeon[1], Daniel R. Rogers[1], Brad M. Bebout[2], John S. Thompson, Jr.[3], and R. Pamela Reid[4]

[1]Department of Marine Sciences, University of Connecticut, Groton, CT 06340
[2]Exobiology Branch, NASA Ames Research Center, Mail Stop 239–4, Moffett Field, CA 94035
[3]University of Miami, University Drive, Coral Gables, FL 33124
[4]Marine Geology and Geophysics, RSMAS – University of Miami, 4600 Rickenbacker Causeway, Miami FL 33149
***Corresponding author: email: Pieter.Visscher@uconn.edu**

Oxygen, sulfide and pH microelectrodes were used to study the biogeochemistry of modern marine stromatolites in the Exuma Cays, Bahamas. Measurements included chemical characterization of the stromatolite mats, both in stagnant water on the beach during a diel cycle as well as short-term *in situ* measurements, and determination of O_2 production and consumption. Experiments with slurried stromatolite mats, in combination with sulfide and/or oxygen electrodes, were used to estimate potential rates of sulfate reduction and sulfide oxidation. Combining these measurements, which are instrumental in the understanding of the microbiology associated with stromatolite formation, facilitate a better biogeochemical interpretation of the formation of these sedimentary structures as well as their ancient ancestors.

Introduction

Stromatolites are lithified laminated sedimentary structures that date back as far as 3.2 Ga (*1,2*) and reached their maximum abundance in the Proterozoic (*3*). Stromatolites are used as evidence for Archean life (*4*) and understanding their biogenic origin may facilitate the search for extraterrestrial life (*5*). The most characteristic feature of stromatolites is the presence of continuous layers of calcium carbonate precipitate that form the lithified layers in these geomicrobiological structures. The presence of alternating lithified and unlithified layers differentiate stromatolites from other microbial mats, the latter which have been studied under the premise that they are analogues of these ancient structures (*6*). Although continuous lithified layers are absent, occasional $CaCO_3$ precipitates are found in these "non-lithifying" analogues (*7,-9)*. Studies in these analogues have implied that cyanobacterial sheath material (*10,11*) and sulfate reducers (*7*) may be involved in the lithification process in stromatolites. Recently, in a study of modern marine stromatolites, Reid et al. (*12*) demonstrated that succession of microbial communities dominated by the cyanobacterium *Schizothrix* sp. are responsible for the observed lithification which ultimately results in the characteristic lamination. Three key communities were recognized in development of lithified and unlithified layers, ranging from a cyanobacterial pioneer community to a climax community with aerobic heterotrophs and sulfate reducers. Copious amounts of amorphous microbial exopolymer, presumably of cyanobacterial origin, and not the more structured sheath material of these organisms, is the key to formation of microcrytalline $CaCO_3$ crusts.

Several key functional groups of microbes that form regular marine and hypersaline mats and modern marine stromatolites are identical and include oxygenic phototrophs, aerobic heterotrophs, sulfate-reducing bacteria (SRB) and sulfide-oxidizing bacteria (SOB) (*12 -15*). Compared to other benthic ecosystems, microbial mats have extremely high rates of oxygenic photosynthesis, aerobic respiration, sulfate reduction and sulfide oxidation (*13,16,17*). The functional groups mentioned above play different roles in the formation of lithified layers (Figure 1): Some contribute to microcrystalline $CaCO_3$ precipitation (oxygenic photosynthesis and sulfate reduction) while others contribute to the dissolution of $CaCO_3$ (aerobic respiration and sulfide oxidation), and may do so in both regular microbial mats and stromatolites.

Microelectrode applications in benthic ecology were pioneered by Teal and Kanwisher (*18*), but did not find a wide application until after Revsbech, Jørgensen and coworkers deployed polarographic oxygen microelectrodes in their studies of laminated microbial mats in Solar Lake, Egypt (*19*), and other locations (*20-22*). Revsbech and coworkers made many improvements in the early electrode design, including development of extremely small sensing tip

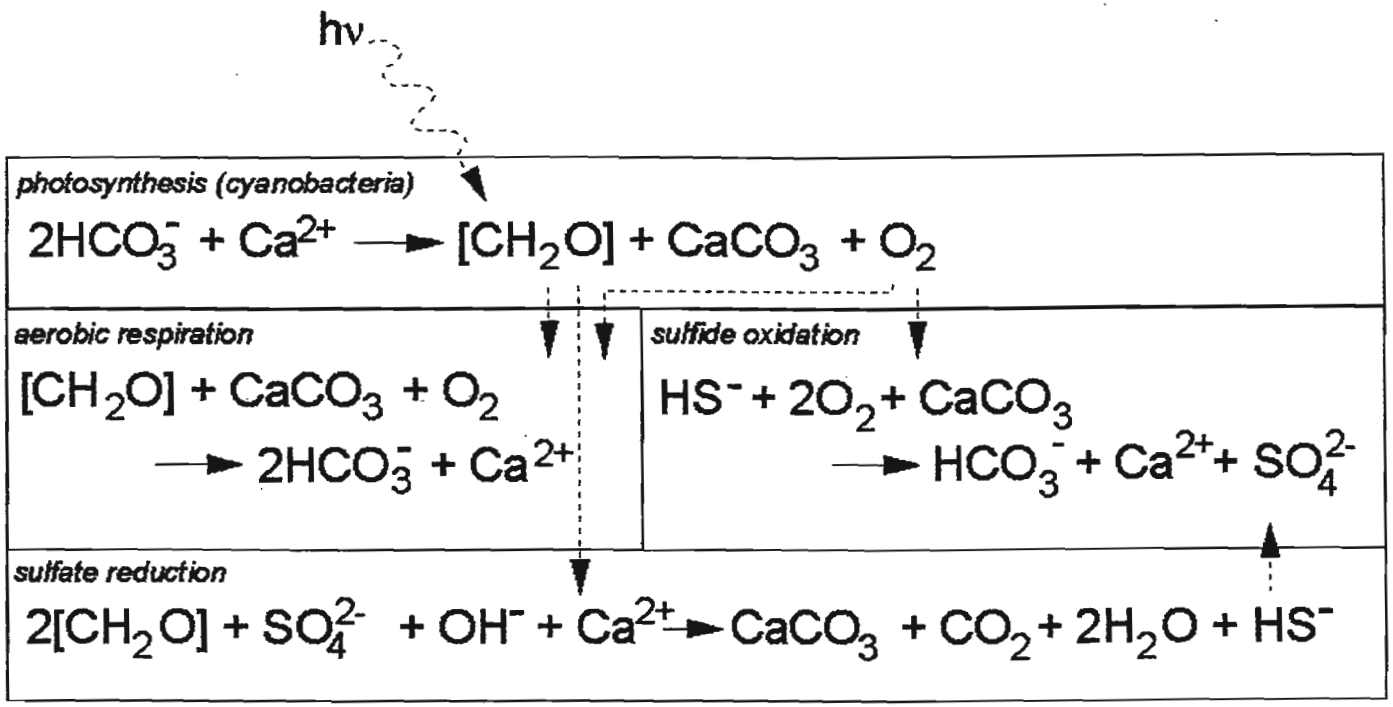

Figure 1. Representation of key microbial processes combined with the geochemical signature as it affects $CaCO_3$ precipitation. Four major functional groups of bacteria in the stromatolite mat are presented. Dashed arrows represent inputs ($h\nu$ is photon energy which drives photosynthesis) and mass transport of key metabolic products ($[CH_2O]$ is the generic formula for photosynthate) as it takes place between the different microbial populations.

dimensions (<10μm) and a guard cathode to allow for a very rapid response time (<0.2 s) minimizing O_2 interferences and reducing the stirring effect (*23*). Electric noise, fluctuating environmental conditions and other technical issues (including fragility of the thin glass sensing tips) in earlier designs resulted in laboratory studies rather than field deployment. Development of stainless steel needle electrodes (outer diameter 0.8 mm) was one of several modifications that enabled measurements *in situ* in a variety of sediment types. In these needle electrodes, the glass has been replaced by epoxy, while the rugged steel casing enables deployment in environments that are hostile to glass electrodes (*24*). There are inherent issues associated with needle electrodes, including dimensions and stirring sensitivity, but the combination of sensing tips for O_2 and S^{2-} in a single needle in combination with the rugged design (*24*) makes these needle electrodes the only suitable tool to obtain depth profiles of O_2 and S^{2-} in lithified structures such as stromatolites.

In this paper, we describe a microelectrode study of modern marine stromatolites using needle and glass microelectrodes for O_2, S^{2-} and pH. In addition to chemical characterization of the stromatolite mat, measurements were carried out to estimate rates of aerobic respiration, sulfate reduction and sulfide oxidation in intact stromatolites and slurried material. Finally, measurements were made *in situ* submerged in approximately 50 cm of water.

Materials and Methods

Site description

Our study was conducted at Highborne Cay, Bahamas, located at the northern end of the Exuma Cays (24°43'N, 76°49'W). Highborne Cay is flanked by Great Bahama Bank on the west and by Exuma Sound on the east. Stromatolites are found on the Exuma Sound side of the island where they occur along a 2 km long beach in between the low tide mark and the fringing reef, which defines the boundary between the shelf and Exuma Sound. Most stromatolites, ranging from 10 cm to several meters, are found in the subtidal area of the shelf. Stromatolite samples were collected from sites NS8 and NS11 (*12,15*). These stromatolites had developed lithified white crusts at their surface, indicative of a "climax" community, that comprises of cynaobacteria (Schizothrix spp, Solentia), aerobic heterotrophic bacteria, SRB and SOB (*12, 15*).

Electrode measurements

The construction and functioning of a variety of microelectrodes has reviewed recently by Glud et al. (*24*). In this study, microelectrode measurements were made with commercially available needle electrodes (Microscale Measurements, Haren, The Netherlands). These probes are built in stainless-steel needles in which the glass has been replaced by epoxy (*25*) as for reason outlined above.

The O_2 needle electrodes consist of an etched Pt-anode with an Au-plated tip (10-20 μm diameter) covered with a cellulose-nitrate membrane, and is polarized at 750 mV negative with respect to a calomel reference electrode. This electrode typically has a 90%-response time of 4-10 s and a drift of approximately 6%-signal min^{-1}. Since the O_2 saturation concentration changes with temperature and salinity, the electrode was calibrated in seawater at the appropriate temperature and salinity (or a range of values of these). Air saturated (100%) values are measured before and after taking readings in the field in seawater bubbled with air for approximately 10 min. The "0%" value is obtained by bubbling with O_2-free N_2 for at least 10 min, the actual concentration checked by a Winkler titration (*26*). The O_2 probe displays a linear response with respect to the ambient O_2 concentration over a wide range (0 to >700% air saturation) (*24,25*), which was tested for 0 and 100% in this study (data not shown). The glass O_2 electrodes with internal reference and guard cathode which were used in this study were obtained commerically (Diamond General, Ann Arbor, MI) with a variety of sensing tip diameters.

The sulfide sensor consists of a silver wire coated with Ag_2S (diameter 100 μm). This sulfide sensor is only sensitive to the fully dissociated form of hydrogen sulfide, S^{2-}, and thus sensitive to the pH of the measuring environment. Under typical seawater conditions, the detection limit is approximately 3-5 μM total sulfide and slightly higher when the pH increases. Calibration was carried out in an airtight vessel containing an oxygen-free buffer of the appropriate pH (7.5, 8.5 and 9.0; see (*25*)), to which incremental amounts of a sulfide stock solution are added. The actual concentration in this calibration solution is checked by the colorimetric methylene-blue method (*27*). The mV decreases 30 mV per decade over a concentration range of 3-3000 μM.

The needle probes deployed in this study included O_2-electrodes, ion-selective sulfide sensors and combined O_2/S^{2-} electrodes (0.8-1 mm outer diameter). Glass Clark-type oxygen microelectrodes with guard cathodes (sensing tip diameter 50 μm) and combined-glass O_2/pH electrodes, all with internal reference electrodes, were obtained from Diamond General (Ann Arbor, MI). Motor-driven stages were used as micromanipulators (MM-3M series, National Aperture, Salem, NH) and were mounted on heavy custom-made PVC adjustable stands. This allows for deployment in up to 15 cm of water and

manipulation of 50-100 μm increments with the aid of a controller box (MC-3B-II, National Aperture, Salem, NH).

In situ underwater measurements in the surf zone were carried out with a hand-driven micromanipulator (model MM33, Märzhäuser-Wetzlar GmbH, Wetzlar, Germany) attached to an Al-stand with additional lead weights to prevent the electrodes from moving in the strong currents. A Keithley model 385 picoammeter with customized variable polarization (Keithley Instruments, Cleveland, OH) or a MasCom ME 01000 meter (MasCom, Bremen, Germany) were used to register the signal of the O_2 electrode and a Microscale Measurements (Haren, The Netherlands) multi-channel high-impedance meter or Beckman F-240 portable pH meter (Fisher Scientific, Pittsburgh, PA) were used to record the signal of S^{2-} and pH electrodes. All meters and micromanipulators were powered by a 12 V deep-cycle marine battery, which allowed for 24-36 h of continuous measurements.

Field Measurements

Diel fluctuations of O_2, pH and S^{2-} were monitored in the upper 25 mm of the stromatolite mat. Profiles were measured every 30 min during daytime and every 60-90 min during nighttime, covering 25 hr in total. In order to avoid submersion of the micromaniopulator, the intact stromatolite head (approximately 20 cm in diamter) was placed in a plastic container, in which void spaces were filled with sand from the location. This restored the stromatolite to an identical condition as experienced prior to sampling. The container with the stromatolite head was kept in *circa* 30 cm of flowing seawater, except when measurements were taken in which case the container was moved to the beach. Measurements were carried out while covered with 2-4 cm of stagnant seawater. The light intensity was registered every 10 min at the beach with a LiCor LI-1000 equipped with a quantum sensor (LiCor, Lincoln, NE). In a separate set of observations *in-situ* was made in a submersed, undisturbed stromatolite. These measurements were carried out during the light period only. The estimate for the flow rate of the water during these measurements was 20-25 cm s^{-1} (*28*). Estimates of oxygenic photosynthesis and aerobic respiration were made by measuring O_2 profiles in the light (1650 μE m^{-2} s^{-1}) followed by measurements taken after the sample and electrode stand were darkened (*20,22,29,30*). The dark profiles were taken for 10 min at 35-68 s intervals. Upon exposure to the light after darkening, O_2 profiles were measured every 45-60 sec for 10 min. The initial changes in the O_2 concentration over time for each depth were calculated from the individual depth profiles.

Shipboard measurements

Measurements under controlled conditions were carried out in a clear PVC flow box in which a water flow of about 5 cm s^{-1} was maintained using a submersible pump. Transient microprofiles were measured upon switching the light intensity from 100 μE m^{-2} s^{-1} to zero using a glass Clark-type electrode with a guard cathode. Profiles of O_2 were measured at 100 μm intervals every 60 s for 23 min. Calculations of aerobic respiration were carried out as outlined above.

Slurry experiments were carried out using either the upper 8-10 mm of the stromatolite or with isolated (individual) lithified layers. This latter approach was chosen since it was demonstrated that the highest microbial metabolic activity was associated with lithified layers (*15*). However, the amount of material required for slurry preparation limited the number of substrates taested for experiments using these individual layers. The stromatolite was dissected and material from lithified layers was homogenized in an equal amount of seawater (1:1 v/v) collected from the site. The 20-ml slurries were incubated in a gastight vessel (no headspace) in which an O_2 and/or S^{2-} electrode was inserted and kept in the dark. The potential for aerobic respiration was determined with a glass oxygen electrode having a guard cathode, and sulfate reduction with a S^{2-} electrode. After obtaining the endogenous O_2 uptake rate for each of the individual slurries, changes in the basal rate of aerobic respiration was calculated from the decrease in O_2 concentration over time upon addition of exogenous organic carbon. Organic carbon sources used included *Schizothrix* exopolymer (EPS), sugars, which are component of the EPS matrix, fatty acids, simple amino acids and alcohols that may result from fermentation and incomplete oxidation and sulfonates which may be part of EPS as well (*31*). Carbon additions were 2-50 μM and O_2 uptake was measured 2-3 times during 15-45 min each and were repeated for at least two concentrations of each exogenous carbon source. The potential for sulfide oxidation was determined by adding sulfide (100-200 μM) and following the decrease in O_2 and S^{2-} concentrations (after 30-60 min preincubation to sequester any free iron), or by adding $S_2O_3^{2-}$ (100 μM) and measuring the decrease in O_2 concentration over time. Molybdate was added to prevent potential microbial sulfide production. The potential rates were calculated from the initial slope of O_2 decrease and S^{2-} increase, for aerobic respiration and sulfate reduction, respectively. Controls for chemical oxidation of carbon and sulfur compounds were carried out for all experiments.

Results

Stromatolite Mat Characterization

Diel measurements of O_2, S^{2-} and pH including two tidal cycles and a diurnal/nocturnal cycle revealed a pattern that is typical for microbial mats: During nighttime, lack of photosynthesis and continued sulfate reduction resulted in anoxic conditions at or close to the surface of the stromatolite (Figure 2). Late in the dark period (2:00-6:00 AM) free sulfide (≥10 μM) was found

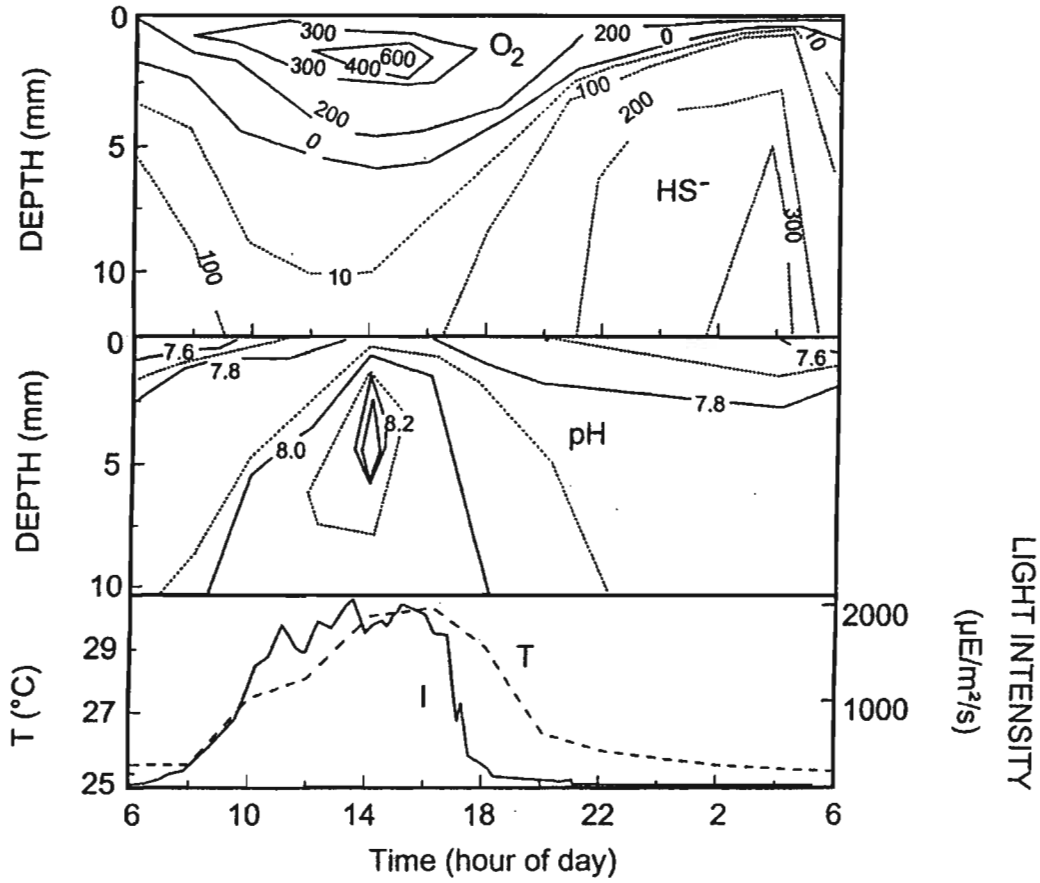

Figure 2. Isopleths of (top panel) the concentration of O_2 (solid lines) and HS^- (dashed lines) in the upper 12 mm of the stromatolite mat; (middle panel) pH (solid lines indicate even decimal pH values, dotted lines odd decimal values); (bottom panel) light intensity (solid lines) and temperature at the surface of the stromatolite (dashed line). Measurements were made on Jun 14-15, 1997, and cover an entire diel cycle.

near the surface at 0.8 mm depth. During the daytime, O_2 production by the cyanobacterial community reestablished an oxic zone in the upper few mm of the stromatolite mat, and appreciable concentrations of sulfide were found only in deeper layers due to chemical and microbial oxidation in the surface of the mats. During the early afternoon, between 8:00 and 4:00 PM, O_2 reaches supersaturation, with peak values of 600-650 μM at 1.5-2 mm depth between 11:30am and 2:45pm. Although the measurements shown in Figure 2 were carried out at the site, thus exposing the sample to natural illumination, they were performed in stagnant water and therefore deviated from true *in situ* conditions. An additional serie of measurements was taken *in situ* in ca. 50 cm of water under a relatively high hydrodynamic flow regime. The large number of particles (ooids) in the water column contributed to extensive light scatter, which may have lead to lower light intensity at the surface of the stromatolite mat. *In situ* measurements were carried out under high tidal flow conditions, which contributed to the observed deeper oxygen penetration and also a lower maximum O_2 concentration (Figure 3). The somewhat rougher shape of the profiles measured *in situ* as opposed to those measured in quiescent water may be caused by stress on the needle probe due to the high flow velocity. Alternatively, this could be caused by the pumping effect of the periodically breaking waves and accompanied entrainment of ooids in the water column resulting in fluctuating light.

Production and Consumption of Oxygen

Rates of photosynthesis and aerobic respiration, estimated from transient O_2 profiles, displayed an increase with depth in the upper mm of the mat, followed by a decrease (Figure 4). Photosynthetic production peaked at a rate of 56 μM O_2 min^{-1} at the 0.5-0.75 mm depth interval. Aerobic respiration rates were lower and peaked at greater depth: 32 μM O_2 min^{-1} at 1-1.25 mm depth. Measurements with glass electrodes resulted in a comparable profile although with a much higher spatial resolution. Also, the rates determined with the thinner glass electrodes were 33-200% higher than those calculated from needle electrode measurements. The needle electrode measurements were carried out under natural light conditions, which were higher than those used during shipboard measurement with glass electrodes. Needle electrodes are known to have a higher O_2 consumption than glass electrodes due to a thicker sensing tip. Despite this, estimations of aerobic respiration were very similar for needle and glass electrodes (Figure 4).

Slurry Experiments

The addition of organic carbon to a slurried stromatolite mat stimulated microbial activity resulting in increase of up to 25 and 15 times for aerobic

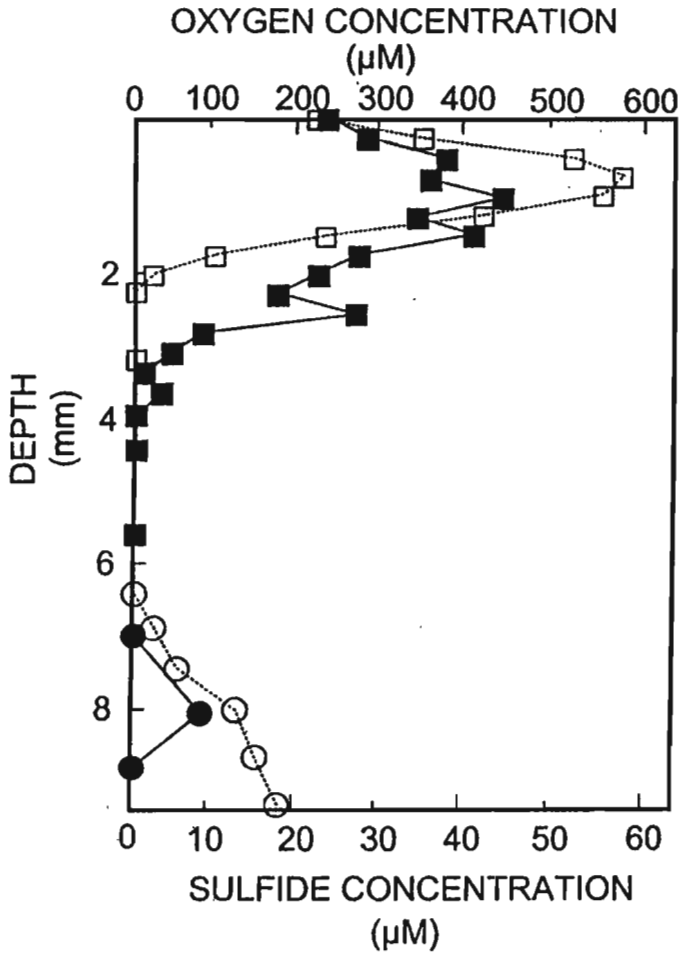

Figure 3. Depth profiles of O_2 and HS^- measured in a stromatolite mat. Squares represent $[O_2]$ and circles $[HS^-]$. Open symbols depict measurements in stagnant water on the beach, closed symbols are in situ *measurements made in approximately 50 cm of water. Dashed lines indicate the approximate depths of lithified (0-0.5 mm and 3-4.5 mm) and unlithified (0.5-3 mm) layers.*

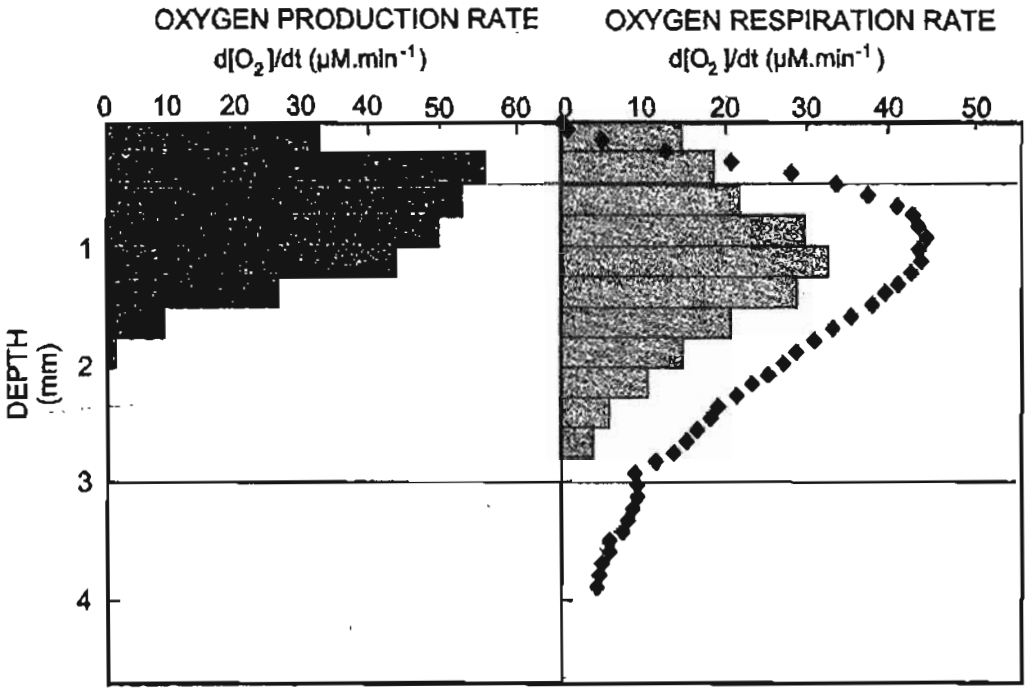

Figure 4. Rates of photosynthesis (left panel) and aerobic respiration (right panel) determined from transient O_2 profiles. Right panel shows a comparison of calculations using needle and glass electrodes, respectively. Bars indicate measurements at the beach in stagnant water under natural illumination (ca. 1600-1800 µM m^{-2} s^{-1}) using needle electrodes, diamonds represent measurements in the laboratory in flowing water using a glass microelectrode.

Table I. Potential rates of aerobic respiration (i.e., O_2 uptake) and sulfate reduction (i.e., S^{2-} production) by bacteria in stromatolite homogenate. Changes in O_2 and HS^- concentration over time were measured with a glass microelectrode with a guard cathode and needle electrode, respectively. EPS = Schizothrix exopolymer (1.67 $\mu g.ml^{-1}$). Listed are the mean and in parenthesis the standard deviation.

Carbon source	Aerobic respiration potential $d[O_2]/dt$ ($\mu mol.ml^{-1}.h^{-1}$)	Sulfate reduction potential $d[S^{2-}]/dt$ ($\mu mol.ml^{-1}.h^{-1}$)
Acetate	158 (14)	127 (8)
Lactate	142 (9)	79 (11)
Ethanol	119 (6)	64 (8)
Glycolate	97 (7)	38 (5)
EPS	48 (11)	32 (6)
Glucose	93 (2)	34 (3)
Mannose	NT*	22 (4)
Xylose	53 (5)	14 (3)
Arabinose	41 (8)	16 (6)
Taurine	38 (8)	35 (2)
Cysteate	NT	24(3)
2-Sulfobenzoate	NT	13 (2)
Glutamate	56 (4)	30 (3)
Endogenous rate	6(1)	8 (1)

*NT = not tested

respiration and sulfate reduction, respectively (Table I). Acetate stimulated both respiratory modes by approximately a factor of 10-20, but more complex molecules, such as sulfonates and the C-6 sugar mannose and C-5 sugar xylose, had a much smaller effect. Interestingly, exopolymer isolated from laboratory cultures of the cyanobacterium *Schizothrix* stimulated respiration more than most of the sugars that could be part of the EPS backbone structure (*31*) and had a similar stimulatory effect on sulfate reduction and on aerobic respiration. Sulfonates stimulated both aerobic and anaerobic respiration, similar to earlier findings (*32*). In an experimental comparison, addition of substrate resulted in a greater stimulation of both aerobic respiration and sulfate reduction in the surface lithified layer, relative to the first sub-surface lithified layer. (Table II). Thiosulfate oxidation rates were higher than rates of sulfide oxidation and both

Table II. Comparison of microbial activity in surface lithified layer (0-1 mm) and next lithified layer (approximately from 4 to 7 mm depth). Potential activities were determined in slurried stromatolite samples.

Carbon source	Surface lithified layer		Sub-surface lithified layer	
	Aerobic respiration potential $d[O_2]/dt$	Sulfate Reduction potential $d[S^{2-}]/dt$	Aerobic respiration potential $d[O_2]/dt$	Sulfate reduction potential $d[S^{2-}]/dt$
Acetate	168 (22)	94 (12)	76 (10)	114 (9)
Ethanol	147 (14)	51 (7)	24 (5)	81 (8)
Glycolate	73 (7)	48 (12)	23 (5)	17 (4)
Endogenous	6 (1)	6 (2)	2 (1)	9 (3)

NOTE: Units are $\mu mol.ml^{-1}.h^{-1}$

were unaffected by the addition of molybdate, an inhibitor of sulfate reduction (Table III). When comparing decreases in O_2 and S^{2-}, sulfide oxidation was incomplete, i.e. there was not a stoichiometric conversion from sulfide to sulfate.

Discussion

Microelectrodes have been applied in studies of microbial mats to understand the dynamics of O_2 production and consumption (*22,24,30,33*). The diel pattern of fluctuating O_2 observed in modern marine stromatolite mats (Figure 2) is not different from similar studies in unlithified microbial mats (*34,35*), although the stromatolite mat differed in that the maximum O_2 concentration was lower: 600 μM versus >1400μM for Solar Lake mats (*34*), and was reached later: between 12:00 noon and 2:00pm versus mid morning in other mats (*34,35*). Likewise, the pH values in most microbial mat studies, including the present, follow the O_2 concentrations and peak when oxygen concentrations are the highest (*14,34*). It is noteworthy that pH values higher than 10 have been reported for unlithifying mats (*37*), in contrast to values of 8.9 in the current study.

Table III. Potential rate of aerobic sulfide and thiosulfate oxidation by sulfide-oxidizing bacteria in slurried stromatolite samples.

Treatment	*HS^- oxidation rate*		*$S_2O_3^{2-}$ oxidation rate*
	$d[O_2]/dt$ ($\mu mol.ml^{-1}.h^{-1}$)	$d[S^{2-}]/dt$ ($\mu mol.ml^{-1}.h^{-1}$)	$d[O_2]/dt$ ($\mu mol.ml^{-1}.h^{-1}$)
Rate upon electron donor addition	45 (6)	41 (4)	87 (12)
Molybdate	43 (8)	48 (6)	81 (8)
Exogenous rate	12 (3)	5(2)	2(1)

Coinciding maximum values of pH and [O_2] are contributed to the extremely high rates of photosynthesis and hence CO_2 consumption, which result in a shift of the carbonate equilibrium and a subsequent increase of the pH. The pattern of S^{2-} distribution followed the typical image with respect to the O_2 isopleths: low (<10μM) sulfide concentrations are found near the surface and increase with depth during the night when O_2 penetration is shallow but the presence of S^{2-} is confined to greater depth during daytime when O_2 reaches higher values and penetrates deeper.

Whereas diel fluctuations are nearly identical in unlithified benthic mats and the modern marine stromatolite mats in the present study, the maximum values of [O_2], pH, [S^{2-}] are lower in the latter. This is also reflected in the activities of key functional groups: photosynthetic rates as calculated from light and dark profiles were at least one order of magnitude lower in the stromatolite when compared hotspring mats (*22*) or temperate marine microbial mats (*30,37*). This lower photosynthetic activity is further confirmed by the lower maximum pH values observed in stromatolite mats compared to non-lithifying mats. Similarly, aerobic respiration was one order of magnitude lower. It should be noted that the stromatolite mats required the use of more rugged needle electrodes versus the unlithified mats. The needle electrodes have less favorable characteristics for applying the transient oxygen microprofiles technique (*30*) (a larger outer dimension, a longer response time and greater sensitivity to stirring). The measurements obtained with Clark-type glass microelectrodes with a guard cathode resulted in higher aerobic respiration rates (Figure 4), which suggest a less pronounced difference between the Bahamian stromatolite mats and other non-lithifying mats (*20,22,30*). However, the difference in microbial activity was shown by traditional measurements of sulfate reduction rates using ^{35}S radiolabel: stromatolite mats sustained maximum rates of 20-35 μM h^{-1} (*32,36*) whereas rates ranging from 27 to 588 μM h^{-1} were reported for unlithified mats (*16,17,38*). It should be noted that the hydrodynamic regime affects the depth profiles (Figure 3) (*39*), and thus the actual *in situ* microbial activities may differ from values calculated in this study.

Interestingly, our measurements of potential microbial metabolic activities in general and sulfate reduction in particular show considerably less of a difference in rates. Potential rates of aerobic respiration and sulfate reduction measured in stromatolite mat slurries are similar to those measured in temperate mats (Tables I, II, III) (*15,32*). It is tempting to speculate, therefore, that actual rates in the stromatolite mat are limited by the availability of organic carbon

produced by oxygenic photosynthesis. This notion is consistent with the observed lower rates of photosynthesis discussed above. Unfortunately, there are few published studies in which electrodes are used to assess the potential of aerobic respiration, sulfate reduction and sulfide oxidation. The low concentrations of Fe in Bahamian waters (*40*) allow for the use of S^{2-} electrodes to measure potential rates of sulfate reduction and sulfide oxidation. However, the Fe-buffering potential of typical shallow benthic sediments (*41*) makes this technique of limited use.

As mentioned above, although $CaCO_3$ precipitates are occasionally observed in non lithifying mats, they only form continuous layers in stromatolites. In a conceptual model for stromatolite mat functioning, decoupling of the four key metabolic reactions outlined in Figure 1, in both time and space would ultimately determine the location and thickness of micritic $CaCO_3$ precipitates (*15*). Some of these micritic layers are further lithified through the boring activity of the endolithic cyanobacterium *Solentia* sp. (*42*). Lack of biomass and hence organic matter in the unlithified layers of stromatolites could possibly result in slightly higher mass transport than typical microbial mat sediments, but more so, both the thin micritic and the thicker lithified layers may form mass transport barriers. Therefore, it can be hypothesized that the physical sedimentological structure of stromatolites allow for a more pronounced decoupling of sulfate reduction and sulfide oxidation, which ultimately could result in the observed continuous $CaCO_3$ precipitates in stromatolites. These observations in modern marine stromatolites may aid in understanding of biotic and abiotic processes that formed Archean stromatolites. Clearly, needle microelectrodes are a crucial tool in the interpretation of the role various microbes play in geomicrobial processes in these lthified microbial mats.

Acknowledgements

This study was supported by NSF grant OCE 9619314 to PTV, Grants from NASA's Exobiology and Astrobiology Missions and Technology Programs to BMB and NSF grant OCE 9530215 to RPR. We thank Dr. R.N. Glud for valuable comments. This is RIBS contribution number 14.

References

1. Walter, M.R.; Buick, R.; Dunlop, J.S.R. *Nature* **1980,** *284,* 443-445.
2. Bertrand-Sarfati, J.; Awramik, S.M. *Bull. Geol. Soc. Am.* **1992,** *104(9),* 1138-1155.

3. Semikhatov, M.A.; Raaben, M.E. In *Microbial Sediments*; Riding, R.E.; Awramik, S.M., Eds.; Springer Verlag: Berlin, Germany, **2000**, pp. 295-314.
4. Hofmann, H.J. In *Microbial Sediments*; Riding, R.E.; Awramik, S.M., Eds.; Springer Verlag: Berlin, Germany, **2000**, pp. 315-327.
5. Farmer, J.D.; DesMarais, D.J. *Lunar Planet Sci. Conf.* **1994**, *25*, 367-368.
6. Awramik, S.M. In *Microbial mats: Stromatolites*; Y. Cohen, Y.; Castenholz, R.W.; Halvorson, H.O. Eds. Alan Liss, New York, NY, **1984**, pp.1-22.
7. Lyons, W.B.; Long, D.T.; Hines, M.E.; Gaudette, H.E.; Armstrong, P.B. *Geology* **1984**, *12*, 623-626.
8. Farmer, J.D. Arizona State University, personal communication, **2000**.
9. Rogers, D.R. University of Connecticut, personal observation, **1999**.
10. Monty, C.L.V. In *Stromatolites*; Walter, M.R. Ed.; Elsevier, Amsterdam, **1976**, pp. 193-249.
11. Chafetz, H.S.; Buczynski, C. *Palaios* **1992**, *7*, 277-293.
12. Reid, R.P.; Visscher, P.T.; Decho, A.W.; Stolz, J.; Bebout, B.M.; Macintyre, I.G.; Paerl, H.W.; Pinckney, J.L.; Prufert-Bebout, L.; Steppe, T.F.; DesMarais, D.J. *Nature* **2000**, *406*, 989-992.
13. Van Gemerden, H. *Mar. Geol.* **1993**, *113*, 3-25.
14. Visscher, P. T.; Van Gemerden, H. In *Biogeochemistry of Global Change: Radiatively Active Trace Gases.* Oremland, R.S. Ed.; Chapman and Hall, New York, NY, **1993**, pp. 672-693.
15. Visscher, P.T.; Reid, R.P.; Bebout, B.M.; Hoeft, S.E.; Macintyre, I.G.; Thompson, J.A. Jr. *Am. Mineral.* **1998**, *83*, 1482-1494.
16. Canfield, D.E.; DesMarais, D.J. *Science* **1991**, *251*, 1471-1473.
17. Visscher, P. T.; Prins, R. A.; Van Gemerden, H. *FEMS Microbiol. Ecol.* **1992**, *86*, 283-294.
18. Teal, J.M.; Kanwisher, J. *Limnol. Oceanogr.* **1961**, *6*, 388-399.
19. Jørgensen, B.B.; Cohen, Y. *Limnol. Oceanogr.* **1977**, *22*, 657-666.
20. Jørgensen, B.B.; Revsbech, N.P.; Blackburn, T.H.; Cohen, Y. *Appl. Environ. Microbiol.* **1979**, *38*, 46-58.
21. Jørgensen, B.B.; Revsbech, N.P.; Cohen, Y. *Limnol. Oceanogr.* **1983**, *28*, 1075-1093.
22. Revsbech, N.P.; Ward, D.M. *Appl. Environ. Microbiol.* **1984**, *48*, 270-278.
23. Revsbech, N.P. *Limnol. Oceanogr.* **1989**, *34*, 472-476.
24. Glud, R.N.: Gundersen, J.K.; Ramsing, N.B. In *In situ monitoring of Aquatic Systems: Chemical Analyis and Speciation;* Buffle, J.; Horvai, G. Eds.; John Wiley & Sons, New York, **2000**, pp.19-73
25. Visscher, P.T.; Beukema, J.; Van Gemerden, H. *Limnol. Oceanogr.* **1991**, *36*, 1476-1480.

26. *A manual of Chemical and Biological Methods for Seawater Analysis*; Parsons, T.R.; Maita, Y.; Lalli, C.M., Eds.; Pergamon, Oxford, England, **1984**, pp.135-141.
27. Cline, J.D. *Limnol. Oceanogr.* **1969,** *14,* 454-458.
28. Huettel, M., Max Planck Inst Marine Microbiol, personal communication, **2000**.
29. Glud, R.N.; Ramsing, N.B.; Revsbech. N.P. *J. Phycol.* **1992,** *28,* 51-60.
30. Epping, E.H.G.; Khalili, A.; Thar, R. *Limnol. Oceanogr.* **1999,** *44,* 1936-1948.
31. Decho, A.W. Oceanogr. Mar. Biol. Ann. Rev. **1990,** 28, 73-154.
32. Visscher, P.T.; Gritzer, R.F.; Leadbetter, E.R. *Appl. Environ. Microbiol.* **1999,** *65*, 3272-3278.
33. Revsbech, N.P.; Jørgensen, B.B. *Adv. Microb. Ecol.* **1986,** *9*, 293-352.
34. Revsbech, N.P.; Jørgensen, B.B.; Blackburn, T.H.; Cohen, Y. *Limnol. Oceanogr.* **1983,** *28*, 1062-1074.
35. Visscher, P.T.; Van den Ende, F.P. In *Microbial Mats. Structure, Development and Environmental Significance;* Stal, L.J.; Caumette, P. Eds.; Springer Verlag, Berlin, Germany, **1994,** pp. 353-360.
36. Visscher, P.T.; Reid, R.P.; Bebout, B.M. *Geology* **2000,** *28*, 919-922.
37. Visscher, P.T.; Quist, P.;Van Gemerden, H. *Appl. Environ. Microbiol.* **1991**, *57*,1758-1763
38. Fründ, C.; Cohen, Y. *Appl. Environ. Microbiol.* **1992,** *58,* 70-77.
39. Ziebis, W.; Huettel, M.; Foster, S. *Mar. Ecol. Progres. Ser.* **1996,** *140*, 227-237.
40. Till, R. *J. Sed. Petrol.* **1970**, *40*(1), 367-385.
41. Heijs, S.K.; Jonkers, H.M.; Van Gemerden, H.; Schaub, B.E.M.; Stal, L.J. *Estuar. Coast. Shelf Sci.* **1999,** *49,* 21-35.
42. MacIntyre, I.G.; Prufert-Bebout, L.; Reid, R.P. *Sediment.* **2000**, *47*, 915-921.